Impulsively Induced Jets from Viscoelastic Films for High-Resolution Printing

Emre Turkoz, Antonio Perazzo, Hyoungsoo Kim, Howard A. Stone, and Craig B. Arnold

Phys. Rev. Lett. **120**, 074501 — Published 15 February 2018

DOI: 10.1103/PhysRevLett.120.074501

Impulsively induced jets from viscoelastic films for high-resolution printing

Emre Turkoz, Antonio Perazzo, Hyoungsoo Kim, Howard A. Stone, and Craig B. Arnold*
Department of Mechanical and Aerospace Engineering, Princeton University, Princeton, NJ, 08544

Understanding jet formation from non-Newtonian fluids is important to improve the quality of various printing and dispensing techniques. Here, we use a laser-based nozzle-less method to investigate impulsively formed jets of non-Newtonian fluids. Experiments with a time-resolved imaging setup demonstrate multiple regimes during jet formation that can result in zero, single or multiple drops per laser pulse. These regimes depend on the ink thickness, ink rheology, and laser energy. For optimized printing it is desirable to select parameters that result in a single-drop breakup, however, the strain-rate dependent rheology of these inks makes it challenging to determine these conditions *a priori*. Rather, we present a methodology to characterize these regimes using dimensionless parameters evaluated from the process parameters and measured ink rheology that are obtained prior to printing and so offer a criterion for single-drop breakup.

Liquid jet formation and subsequent breakup to form droplets depend on the interplay among the elastic, inertial, capillary, and viscous effects [1–3]. The underlying forces also dictate whether a liquid filament will result in multiple, single or zero droplets [4, 5]. While the behavior of jets from Newtonian fluids (Newtonian jets) and drop formation are more predictable with the well-understood Rayleigh-Plateau [6, 7] instability, it is observed that jets from non-Newtonian fluids (non-Newtonian jets) generally exhibit different structures compared to Newtonian jets due to their strain-rate dependent rheology and inherent viscoelasticity and/or viscoplasticity. An example of this phenomenon for non-Newtonian jets is the observation of "beads-on-a-string" formation, which refers to a nearly periodic arrangement of drops connected along an unbroken but narrow polymeric thread [8, 9]. Modeling of the "beads-on-a-string" dynamics showed that a low ratio of the viscous to inertia-capillary time scales (or Ohnesorge number) [10–12] and aspect ratios larger than a critical value for a given polymer [13] enhance bead formation. Such structures on non-Newtonian jets should be understood and controlled, if possible, for a given engineering application.

In this Letter, we investigate the formation of jets from viscoelastic dilute polymer solutions. In particular, we seek to identify a methodology to determine the optimum printing conditions to yield single-drop breakup following formation of a jet. As an experimental technique, blister-actuated laser induced forward transfer (BA-LIFT) is used [14]. BA-LIFT has been developed as a nozzle-less printing technique in which a laser pulse is absorbed by an interfacial layer that forms a rapidly growing blister (figure 1a), where the blister results from the plastic deformation on the polyimide layer [15]. This technique, along with other LIFT variants, has been used extensively for the printing of technologically relevant materials [16–19]. Studies on BA-LIFT found that after the rapid formation of the blister and the transfer of the kinetic energy to the fluid, a jet starts to form normal to the blister due to the inertial forcing, and the surrounding fluid is pulled from the vicinity of the blister towards its center [20, 21]. This phenomenon makes BA-LIFT a useful platform to investigate non-Newtonian inks, because the rheology of these materials changes depending on the applied strain-rate. A typical blister generated using the BA-LIFT experimental setup (figure 1a) has a Gaussian-like profile as shown in figure 1b. In this study, two different energy levels are used to generate blisters, with the shape profiles of these blisters presented in figure 1c. The formation of a jet and material transfer depend on the combination of experimental parameters including laser energy, ink layer thickness and the rheology of the material to be printed.

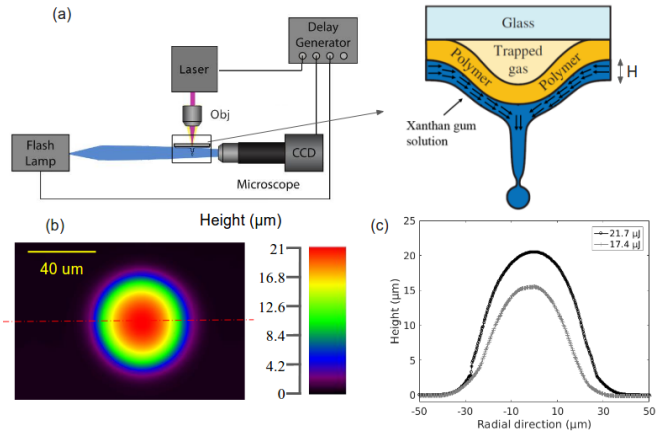

FIG. 1. BA-LIFT experimental setup and blister formation. (a) A schematic of the experimental setup of BA-LIFT along with the representation of the substrate and blister formation. The ink with thickness H in the vicinity of the blister undergoes shear flow to form the jet. (b) A contour plot of a 21.7 μJ blister profile as it appears under the confocal microscope. The dashed red line is the centerline of the blister. (c) Blister profiles created with high and low energies.

Xanthan gum solutions, which exhibit shear-thinning and viscoelastic behavior similar to inks such as silver pastes [22], are chosen as a model ink to investigate the jetting behavior. Solutions are prepared with five different xanthan gum concentrations [XG]: 0.05, 0.1, 0.2,

0.4, and 0.8 wt.% in water and water-glycerol mixtures. Representative results of viscosity versus shear rate from shear rheology measurements are presented in figure 2a. The dependence on shear rate for the viscosities of these solutions can be expressed with a power law in the form of $\mu(\dot{\gamma}) = a\dot{\gamma}^n$. We measure the viscoelastic relaxation time λ from the diameter-thinning dynamics of a gravity jet [23] as depicted in figure 2b. In this figure, the time axis denotes the time before the pinch-off of the jet ($t_0 - t$) and the filament diameter (D_{min}) is the smallest diameter along the filament (see the inset of figure 2b). During pinch-off, the exponential part of the curve can be fitted with the profile $D_{min} \propto \exp(\frac{1}{3\lambda}(t_0 - t))$ [23, 24], which allows an estimate of λ. Increasing polymer concentration results in longer relaxation times, as expected [25]; the relaxation time remains almost the same for different ratios of water and glycerol [26].

In our BA-LIFT experiments, five different jetting and drop formation regimes are observed from time-resolved imaging results. One of these regimes is the "no jetting" regime, where the supplied energy to the fluid is insufficient for jet formation. Figure 3a presents the jetting without breakup regime where the incident laser energy is high enough to initiate the jet formation, however it is insufficient for the jet go through pinch-off [27]. This limiting behavior is a consequence of a combination of the viscoelastic effects that result from the resistance of polymer chains to extension, and surface tension that resists the propagation of a filament due to the creation of new surface. The "multiple-drop breakup" regime is shown in figure 3b. For viscoelastic fluids, sometimes this response has been referred in the literature [9] as "beads-on-a-string" (BOAS) breakup. Since the BOAS regime results in multiple droplets transferred to a substrate, it is not desirable for high-resolution printing [28]. Also, a turbulent-like regime is observed as shown in figure 3c, which was recently identified as ligament-mediated fragmentation [29] and results in a spray-like ejection process and gets completed before a uniform jet is formed.

Single-drop pinch-off is depicted in figure 3d. It is the most desirable operating regime for printing. We observe that higher xanthan gum concentrations with small ink layer thicknesses result in single-drop pinch-off, while lower polymer concentrations allow for the formation of multiple drops. Figure 4a shows the distribution of the five jetting regimes with changing xanthan gum concentration for water-based solutions.

The governing forces and the observed dynamical regimes are better understood when the dimensionless parameters are evaluated. The time scales of the forces for jet formation derive from elastic, the inertia-capillary, and visco-capillary effects. The elastic time scale is characterized by the relaxation time λ, which is evaluated as described above. The inertia-capillary time scale can be defined as $t_c = \sqrt{\rho H^3/\sigma} = \sqrt{0.118}/\omega_R$, where σ denotes the surface tension, ρ is the density of the fluid, and H is

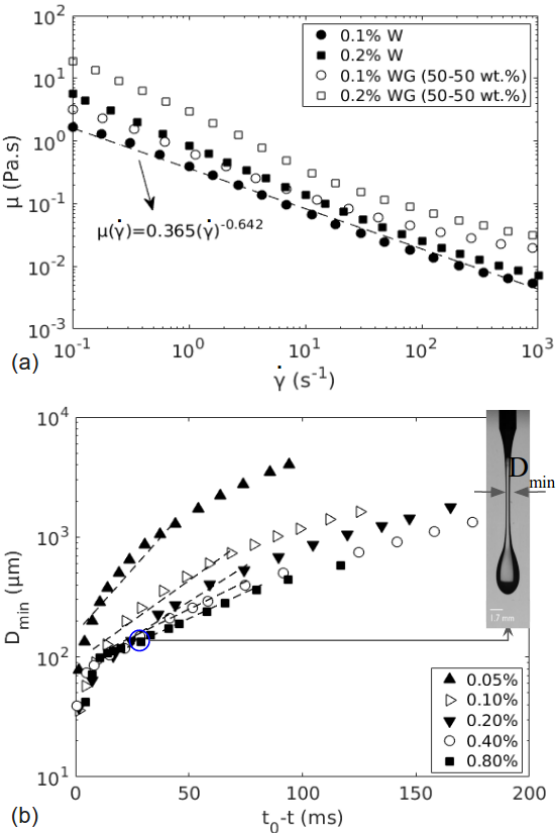

FIG. 2. Shear and elongational rheometry of xanthan gum solutions. (a) Shear viscosity (μ) of 0.1 wt.% and 0.2 wt.% [XG] with water (W) and water-glycerol (WG 50-50 wt.%) mixtures as a function of shear rate ($\dot{\gamma}$). (b) Change of the minimum diameter (D_{min}) of gravity-driven jets (inset) created using different [XG] with water as the solvent plotted against the time before pinch-off ($t_0 - t$), where t_0 denotes the pinch-off time. The exponential fits $D_{min} \propto \exp(\frac{1}{3\lambda}(t_0 - t))$ are performed on the curves during thinning before pinch-off and shown as dashed lines. The smallest and largest relaxation times are evaluated as 6.8 ms (0.05 wt.%) and 18 ms (0.8 wt.%), respectively. The complete list of values is presented in [26].

the ink layer thickness, which is proportional to the jet radius [26, 30], and ω_R defines the conventional Rayleigh capillary instability growth rate [31]. The visco-capillary time scale [1] is defined as $t_v = \mu_0 H/\sigma$, where μ_0 denotes the zero shear viscosity.

The Ohnesorge, $Oh = \mu_0/\sqrt{\rho\sigma H}$, and Deborah $De = \lambda\omega_R$, numbers have been used in the literature [11, 30] to compare the relative effects of the underlying forces. Previous studies have considered the zero-shear viscosity for the viscous time scale while evaluating the Ohnesorge number [32]. However, in thin-film configurations with BA-LIFT, analytical and numerical studies of the early time dynamics show that the fluid pulled from the sides experiences shear [21], so the effective shear viscosity should be changed accordingly using the rheological

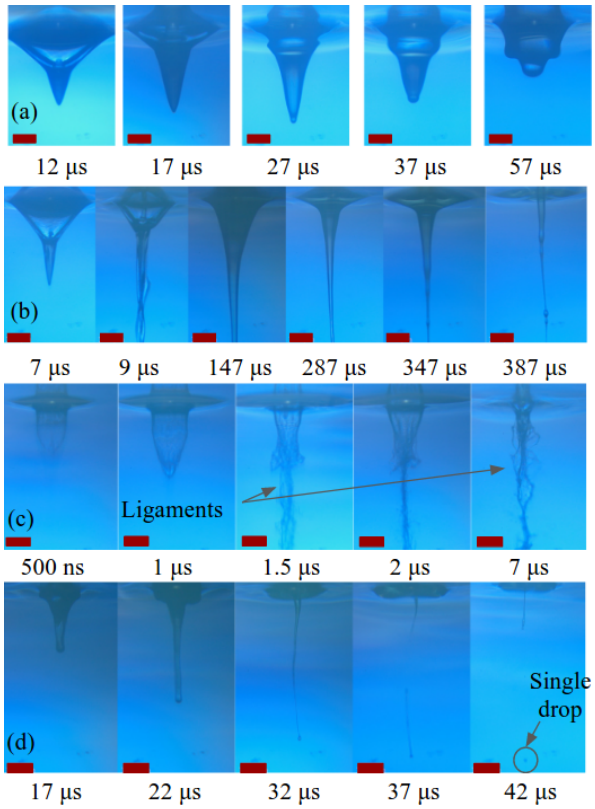

FIG. 3. Different jetting regimes observed in BA-LIFT experiments with high-energy (21.7 μJ) blisters. (a) Jetting without breakup. (b) Multiple-drop breakup. (c) Ligament-mediated fragmentation. (d) Single-drop breakup. Scale bars represent 100 μm.

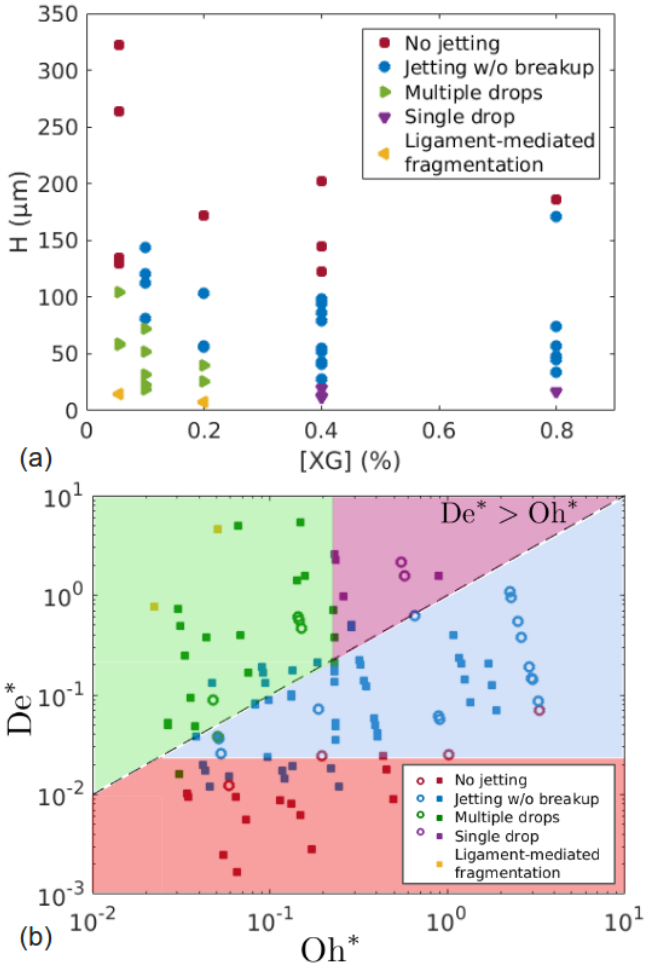

FIG. 4. Ink thickness, xanthan gum concentration, and laser energy affect the resulting regime. (a) Different regimes obtained for solutions with water solvents changing with xanthan gum concentration ([XG]) and ink thickness (H) for the high-energy blister (21.7 μJ). (b) A plot of De^* versus Oh^*, where $De^* = \lambda\omega_R(U_c/U_b)$ with $U_c = \sqrt{\sigma/\rho H}$ and U_b is the average blister velocity depending on the laser energy [26]. $De^* = Oh^*$ line divides the regimes with breakup from the regimes without breakup. Different colors represent different regimes as shown in the legend of the plot. Squares (■) represent data obtained with higher laser energy (21.7 μJ), whereas circles (o) represent data obtained with lower laser energy (17.4 μJ).

data. We address this problem by evaluating a characteristic shear rate ($\dot{\gamma}_{ch}$) from analytical energy and mass balances defined for the blister (figure 5). We define U_b as the time and space-averaged blister velocity, ΔV_b is the volume of the blister evaluated using numerical integration from the profile obtained using confocal microscopy, μ_{el} is the elongational viscosity whose evaluation is explained in [26], H_b is the blister height, U_{jet} is the velocity of the jet in the normal direction to the fluid layer, $\Delta V = \pi R_b^2 H$ is the volume of the fluid that is assumed to be set into motion, ΔA is the new area created by the deformation of the free surface, U_{shear} is the maximum value of the shear velocity that is assumed to have a linear profile (figure 5), and R_b denotes the blister radius. Then, the energy balance can be written as:

$$\underbrace{\frac{1}{2}\rho U_b^2 \Delta V_b}_{\text{input energy}} - \underbrace{\mu_{el}\frac{U_b}{H_b}\Delta V_b}_{\text{loss due to elongation}} = \underbrace{\frac{1}{2}\rho U_{jet}^2 \Delta V}_{\text{jet kinetic energy}} + \underbrace{\sigma \Delta A}_{\text{interface formation}} + \underbrace{\mu_0 \frac{U_{shear}}{H}\Delta V}_{\text{loss due to shear}}, \quad (1)$$

which is accompanied by an approximate mass balance:

$$U_{jet}\pi R_b^2 = \frac{U_{shear}}{2} 2\pi R_b H\,. \quad (2)$$

In the energy balance (1), the first expression on the left-hand side denotes the kinetic energy supplied to the fluid due to the motion of the blister. We assume that there is a no-slip boundary condition between the moving blister and the fluid that is attached to the solid surface, so that at early times the fluid has the same velocity as the blister. The second term on the left-hand side rep-

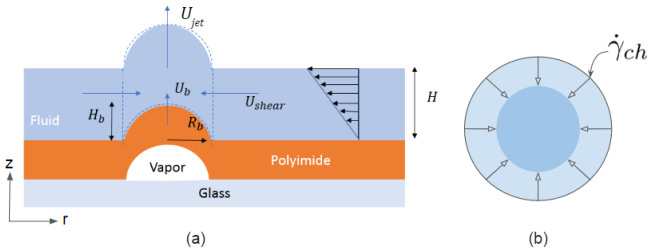

FIG. 5. Jet formation during BA-LIFT. (a) Side view during jet formation. Dashed boundaries define the control volume for the analytical model. (b) Top view of the process. Flow is inward with a characteristic shear rate $\dot{\gamma}_{ch}$.

resents the energy lost to the viscous dissipation with the expansion of the blister. Here it is assumed that the applied stress from the blister on the fluid is in the extensional direction because the blister expands normal to the surface of the polymer. Accordingly, the elongational viscosity (μ_{el}) is included in the analysis with the strain rate given in the normal direction.

The energy remaining after the initial motion and dissipation consists of three different contributions as shown in the right-hand side of (1). The first term on the right-hand side is the kinetic energy of the jet. The second term represents the energy cost of forming new surface area, where ΔA is evaluated numerically from the profile of the blister. The last term is the energy lost to dissipation in an approximate shear flow. Here the viscosity is taken as the zero-shear viscosity, which in turn results in a more conservative estimate of the shear velocity.

The approximate mass balance given in (2) accounts for the mass leaving the control domain with the mean velocity (U_{jet}), and the mass entering the domain from the sides through the cylindrical face of the control volume with the mean velocity ($U_{shear}/2$), where a linear velocity profile across the film was assumed. Using the shear flow speed of the fluid in the vicinity of the blister (U_{shear}) calculated from these balances, the characteristic shear rate is estimated as $\dot{\gamma}_{ch} = U_{shear}/H$. Knowing $\dot{\gamma}_{ch}$, the resulting effective Ohnesorge number Oh^* is evaluated as $Oh^* = t_v^*/t_c = \mu(\dot{\gamma}_{ch})/\sqrt{\rho\sigma H}$, where $\mu(\dot{\gamma}_{ch})$ is the viscosity evaluated with the characteristic shear rate from the rheological data.

While the Deborah number, $De = \lambda\omega_R$, is conventionally used to include the effect of elasticity in the analysis of non-Newtonian filaments [11, 33], it should be noted that De does not include any information that is related to the forcing, which is produced by the rapid expansion of the blister. The forcing directly affects the amount of stretching of the filament, which should be expected to influence the fluid properties. In particular, the viscoelastic filament exhibits larger stresses with stretching, and the effective relaxation time of the polymer solution decreases with increasing strain rate [34, 35]. The relative stretching of a filament can be denoted with the aspect ratio of the jet L_{max}/H, where L_{max} is the jet *intact length* before the breakup. The jet extends until it breaks up at $t_{breakup} \approx t_c$, $H \approx U_c t_{breakup}$ since H is comparable to the jet radius [26], where $U_c = \sqrt{\sigma/\rho H}$ is a typical inertially estimated breakup speed. Also, $L_{max} \approx U_b t_{breakup}$, where U_b is the laser-energy-dependent time and space-averaged blister velocity used as an estimate for the jet velocity in the axial direction, which is a measure of stretching. Since $H/L_{max} \sim U_c/U_b$, we propose a modification to the Deborah number as $De^* = \lambda\omega_R\,(U_c/U_b)$.

The comparison of the two modified dimensionless parameters, De^* and Oh^*, leads to the separation of the observed regimes as shown in figure 4b. For a filament to breakup into droplets, the capillary thinning should overcome the viscous resistance, which leads to the condition $t_c > t_v^*$ or $Oh^* < 1$ as given in the literature for Newtonian filaments [5]. Furthermore, since the viscoelastic filaments produce higher radial stresses as they are stretched, the effective relaxation time can be expected to fulfill the condition $\lambda H/L_{max} > t_v^*$ for the breakup.

The multiple drop regimes can be separated from the single-drop regime by examining the Ohnesorge number [5, 11]. A numerical study [11] recently investigated the thinning of viscoelastic filaments fixed between two circular plates, and multiple drop formation was reported to be suppressed for Oh > 0.5. In our experiments this threshold can be expected to be lower due to the energy dissipated shearing the ink layer in the BA-LIFT configuration.

The region of jetting without breakup can be separated from the no-jetting region by examining the early times of the process prior to jet formation. If the inertial effect is large relative to the deformation caused by the rapidly forming blister, all of the energy is absorbed by the film, and no jet is formed. To check the influence of inertia, the inertia-capillary time scale, t_c, again applies and should be compared with the time scale of the elastic effects, λ. Therefore, the region separating no jetting from jetting without breakup can be roughly described by horizontal $De =$ const. or $De^* =$ const. line (fig. 4b).

Furthermore, the regime diagram presented in fig. 4b shows that the $De^* = Oh^*$ line separates the jetting regimes with breakup from the regimes without breakup. Also, no breakup is observed for $Oh^* > 1$. The $Oh^* \approx 0.2$ line can be used to separate multiple drop regimes from the single-drop regime. In addition, the unmodified Deborah number threshold separating the no jetting from jetting without breakup regimes is evaluated as $De \approx 10$ for the higher laser energy (21.7 μJ), and $De \approx 35$ for the lower laser energy (17.4 μJ). For the single-drop ejection to take place, the three conditions mentioned above, $De^* > Oh^*$, $0.2 < Oh^* < 1$, and $De >$ const., should be satisfied. These dimensionless numbers can be evaluated using the experiment parameters before the printing is

performed, and the criteria presented here can be used to predict the resulting regime of the jetting process, which is crucial for the success of the drop-on-demand deposition techniques. The methodology described in this study can be generalized to other dispensing and printing applications that utilize jets. The general conclusions and guidelines can help enable new high-resolution printing methods with other viscoelastic materials.

We acknowledge Prof. Giovanna Tomaiuolo for the fruitful discussions on oscillatory rheometry.

* Corresponding author:cbarnold@princeton.edu

[1] J. Eggers and E. Villermaux, Reports on Progress in Physics **71**, 036601 (2008).
[2] J. Eggers and M. A. Fontelos, *Singularities: Formation, Structure, and Propagation*, Vol. 53 (Cambridge University Press, 2015).
[3] J. R. Castrejón-Pita, A. A. Castrejón-Pita, S. S. Thete, K. Sambath, I. M. Hutchings, J. Hinch, J. R. Lister, and O. A. Basaran, Proceedings of the National Academy of Sciences **112**, 4582 (2015).
[4] H. A. Stone, Annual Review of Fluid Mechanics **26**, 65 (1994).
[5] A. A. Castrejón-Pita, J. Castrejon-Pita, and I. Hutchings, Physical Review Letters **108**, 074506 (2012).
[6] J. A. F. Plateau, *Statique Expérimentale et Théorique des Liquides Soumis aux Seules Forces Moléculaires*, Vol. 2 (Gauthier-Villars, 1873).
[7] Y. Li and J. E. Sprittles, Journal of Fluid Mechanics **797**, 29 (2016).
[8] J. Li and M. A. Fontelos, Physics of Fluids **15**, 922 (2003).
[9] C. Clasen, J. Eggers, M. A. Fontelos, J. Li, and G. H. McKinley, Journal of Fluid Mechanics **556**, 283 (2006).
[10] A. Ardekani, V. Sharma, and G. McKinley, Journal of Fluid Mechanics **665**, 46 (2010).
[11] P. P. Bhat, S. Appathurai, M. T. Harris, M. Pasquali, G. H. McKinley, and O. A. Basaran, Nature Physics **6**, 625 (2010).
[12] C. McIlroy, O. Harlen, and N. Morrison, Journal of Non-Newtonian Fluid Mechanics **201**, 17 (2013).
[13] J. Eggers, Physics of Fluids **26**, 033106 (2014).
[14] N. T. Kattamis, P. E. Purnick, R. Weiss, and C. B. Arnold, Applied Physics Letters **91**, 171120 (2007).
[15] N. T. Kattamis, M. S. Brown, and C. B. Arnold, Journal of Materials Research **26**, 2438 (2011).
[16] C. B. Arnold, P. Serra, and A. Piqué, MRS Bulletin **32**, 23 (2007).
[17] I. Zergioti, A. Karaiskou, D. Papazoglou, C. Fotakis, M. Kapsetaki, and D. Kafetzopoulos, Applied Physics Letters **86**, 163902 (2005).
[18] J. Wang, R. C. Auyeung, H. Kim, N. A. Charipar, and A. Piqué, Advanced Materials **22**, 4462 (2010).
[19] G. Hennig, T. Baldermann, C. Nussbaum, M. Rossier, A. Brockelt, L. Schuler, and G. Hochstein, Journal of Laser Micro/Nanoengineering **7** (2012).
[20] M. S. Brown, C. F. Brasz, Y. Ventikos, and C. B. Arnold, Journal of Fluid Mechanics **709**, 341 (2012).
[21] C. F. Brasz, C. B. Arnold, H. A. Stone, and J. R. Lister, Journal of Fluid Mechanics **767**, 811 (2015).
[22] D. Munoz-Martin, C. Brasz, Y. Chen, M. Morales, C. Arnold, and C. Molpeceres, Applied Surface Science (2016).
[23] M. Roché, H. Kellay, and H. A. Stone, Physical Review Letters **107**, 134503 (2011).
[24] S. L. Anna and G. H. McKinley, Journal of Rheology **45**, 115 (2001).
[25] J. Dinic, Y. Zhang, L. N. Jimenez, and V. Sharma, ACS Macro Letters **4**, 804 (2015).
[26] See Supplementary Material, which includes detailed rheometry, experimental setup, and information on scaling analysis, which includes Refs. [36-41].
[27] E. Turkoz, L. Deike, and C. B. Arnold, Applied Physics A **123**, 652 (2017).
[28] Z. Zhang, R. Xiong, D. T. Corr, and Y. Huang, Langmuir **32**, 3004 (2016).
[29] B. Keshavarz, E. C. Houze, J. R. Moore, M. R. Koerner, and G. H. McKinley, Physical Review Letters **117**, 154502 (2016).
[30] C. Wagner, Y. Amarouchene, D. Bonn, and J. Eggers, Physical Review Letters **95**, 164504 (2005).
[31] L. Rayleigh, The London, Edinburgh, and Dublin Philosophical Magazine and Journal of Science **34**, 145 (1892).
[32] Z. Zhang, R. Xiong, R. Mei, Y. Huang, and D. B. Chrisey, Langmuir **31**, 6447 (2015).
[33] W. Du, T. Fu, Q. Zhang, C. Zhu, Y. Ma, and H. Z. Li, Chemical Engineering Science **153**, 255 (2016).
[34] P. E. Arratia, G. A. Voth, and J. P. Gollub, Physics of Fluids **17**, 053102 (2005).
[35] J. A. Long, A. Ündar, K. B. Manning, and S. Deutsch, ASAIO journal **51**, 563 (2005).
[36] M. Aytouna, J. Paredes, N. Shahidzadeh-Bonn, S. Moulinet, C. Wagner, Y. Amarouchene, J. Eggers, and D. Bonn, Physical Review Letters **110**, 034501 (2013).
[37] M. Khagram, R. Gupta, and T. Sridhar, Journal of Rheology **29**, 191 (1985).
[38] M. Zirnsak, D. Boger, and V. Tirtaatmadja, Journal of Rheology **43**, 627 (1999).
[39] G. Batchelor, Journal of Fluid Mechanics **46**, 813 (1971).
[40] J. L. Schrag, Transactions of the Society of Rheology **21**, 399 (1977).
[41] G. Thurston and G. Pope, Journal of Non-Newtonian Fluid Mechanics **9**, 69 (1981).